$\begin{array}{l} \textbf{63},\,4,\,\mathrm{pp.}\,\,915–928,\,\mathrm{Warsaw}\,\,2025 \\ \mathrm{https://doi.org/}10.15632/\mathrm{jtam-pl/}208836 \end{array}$ 

# SIMULATED CALCULATION AND APPLICATION OF ANNULAR PRESSURE LOSS FOR DEEP SLIM-HOLE SIDETRACKING HORIZONTAL WELL

Zaiming WANG<sup>1</sup>, Yuanyuan SHEN<sup>1</sup>, Yi HOU<sup>1</sup>, Yanna KAN<sup>1</sup>, Weian HUANG<sup>2\*</sup>, Yuqing ZHU<sup>2</sup>

<sup>1</sup> Production Technology Research Institute, PetroChina Jidong Oilfield Company, Tangshan, China <sup>2</sup> School of Petroleum Engineering, China University of Petroleum (Huadong), Qingdao, China \*corresponding author, masterhuang1997@163.com

This article analyzes the influence of different displacement  $(5\,\mathrm{L/s}\text{-}17\,\mathrm{L/s}$  (liter per second)) and rotational speed  $(0\,\mathrm{rev/min}\text{-}120\,\mathrm{rev/min})$  conditions on the annular pressure loss of a slim hole under different eccentricity  $(0\,\%\text{-}40\,\%)$  models through simulation methods and the difference in the annular pressure drop gradient at different drilling tool combinations. Based on numerical simulation, results fitted the multi-factor dimensionless annular pressure drop gradient factor. The accuracy of the fitted factors was verified by calculating the pump pressure of a horizontal wellbore section based on the historical data of the SY-3 well with an error of less than  $10\,\%$ .

Keywords: slim-hole well; deep sidetracking well; eccentric rotation; annular pressure loss.



Articles in JTAM are published under Creative Commons Attribution 4.0 International. Unported License https://creativecommons.org/licenses/by/4.0/deed.en. By submitting an article for publication, the authors consent to the grant of the said license.

#### 1. Introduction

The shale oil geological resources in the Qintong Depression of the Subei Basin are abundant. The SY-3 well has been deployed in order to explore low-cost engineering processes and promote the efficient development of shale oil. This well was drilled through a discontinued old well with sidetrack drilling, using the horizontal drilling technology of a \$\infty\$118 mm small wellbore. It is the first deep shale oil small wellbore lateral drilling horizontal well in the work area. Due to factors such as small drilling size and small annular clearance, the annular pressure consumption during the drilling process is high, and the formation is prone to collapse and leakage. Therefore, the pump pressure is limited. Moreover, it has a long horizontal segment and a local upward trajectory, which poses a challenge to wellbore cleaning (Delwiche et al., 1992; Song et al., 2004). There are significant differences in hydraulics between slim-hole drilling and conventional wellbore drilling. Therefore, scholars have conducted theoretical and experimental research on the calculation of eccentric rotation annular pressure drop in small wellbore drilling (McCann et al., 1995; Haciislamoglu & Cartalos, 1994; Cartalos et al., 1996; Hansen et al., 1999; Hemphill & Ravi, 2005; Enfis et al., 2011; Kelessidis et al., 2011; Reed & Pilehvari, 1993; Letelier et al., 2017; Tian et al., 2022; Khatibi et al., 2018; Vieira et al., 2014; Sotoudeh & Frigaard, 2024; Shi & Zhang, 2025; Resell et al., 2025). Various computational models have been established, but all of them have limitations, and all of them have some errors in performing prediction calculations. Experimental studies have demanding requirements on the precision of the instruments and the accuracy of the operation. McCann et al. (1995) conducted experimental research on pressure changes in narrow annular spaces, but did not consider the effect of eccentricity. The computational model proposed by Haciishamoglu and Cartalos (1994) and Kelessidis et al. (2011) did not take into account the influencing factors of drill string rotation.

Hansen et al. (1999) did not analyze the gradient changes in annular pressure drop at sudden diameter changes such as drilling tool joints. Khatibi et al. (2018) established a computational model based on experimental research, and did not alter the diameter ratio during the experiment. Sotoudeh and Frigaard (2024) focus on cementing, and the empirical size is not a small wellbore. Resell et al. (2025) investigate fluid forces and viscous torque on an inner cylinder that simultaneously rotates about its own axis and orbits within an outer cylinder. However, they did not establish an expression for annular pressure drop. In this regard, the author combines domestic and international research data on small-borehole technology, and further investigates the effects of eccentricity, rotation, displacement, drilling tool combinations, and other factors on the annular pressure consumption of small boreholes through simulation. The fitted multifactorial uncaused annulus pressure drop gradient factor can provide a reference for calculating the annulus pressure consumption and optimizing the hydraulic parameters for drilling small boreholes.

#### 2. Establishment of annular model for slim hole

# 2.1. Solidworks modeling and fluid domain partitioning

According to the field conditions and drilling design, the commonly used drilling tools combination for drilling in a particular well section is simulated by Solidworks. The simulated pipe string with a length of 25.28 meters is established as  $\varnothing 118\,\mathrm{mm}$  polycrystalline diamond compact bit (PDC) +  $\varnothing 95\,\mathrm{mm}$  measurement while drilling (MWD) +  $\varnothing 73\,\mathrm{mm}$  drill pipe +  $\varnothing 105\,\mathrm{mm}$  joints. The annulus is set to  $\varnothing 150\,\mathrm{mm}$ . The fluid domain is divided by a Boolean operation. The inner pipe column and fluid domain are as shown in Fig. 1.

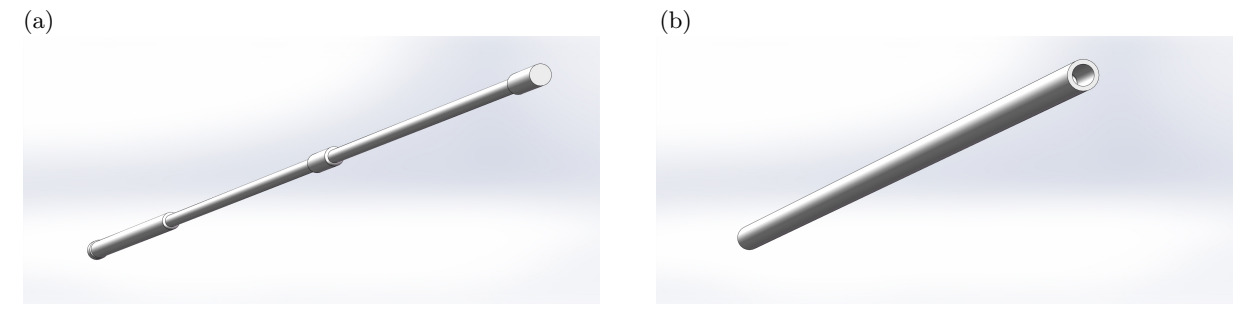


Fig. 1. Inner column and fluid domain: (a) inner pipe; (b) fluid domain.

The eccentricity formula can be expressed as (Tian et al., 2022):

$$E = \frac{\delta}{r_w - r_d},\tag{2.1}$$

where E is the eccentricity,  $\delta$  is the eccentricity distance, which is the distance between the drill bit and the two centers of the wellbore in the view along the axis of the wellbore [m],  $r_w$  is the radius of the wellbore [m], and  $r_d$  is the radius of the drill pipe [m].

The pipe string model is uniformly modeled by Solidworks with five eccentricities: 0% (eccentricity  $0 \, \text{mm}$ ), 10% (eccentricity  $3 \, \text{mm}$ ), 20% (eccentricity  $6 \, \text{mm}$ ), 30% (eccentricity  $9 \, \text{mm}$ ), and 40% (eccentricity  $12 \, \text{mm}$ ), and the eccentricity model is shown in Fig. 2.



Fig. 2. Different eccentricity models: (a) eccentricity 0 %; (b) eccentricity 10 %; (c) eccentricity 20 %; (d) eccentricity 30 %; (e) eccentricity 40 %.

#### 2.2. Fluent meshing and model setup

The model built by Solidworks is imported into Design Modeler, named fluid domain import and export, and structured meshing is performed to accelerate convergence. Taking the 10% eccentricity model as an example, the meshing results are shown in Fig. 3. A total of 245131 faces were divided with a maximum twist of 0.2174 and a maximum aspect ratio of 16.57, and a total of 546482 control body meshes were divided with a minimum orthogonal mass of 0.3056, a maximum aspect ratio of 5.89, and no isolated meshes. The maximum mesh distortion is 0.6944, the minimum distortion is 0.0029, and the average distortion is 0.0476. The mesh quality is excellent, which meets Fluent's requirements for the mesh quality, and is conducive to the convergence of the calculation.

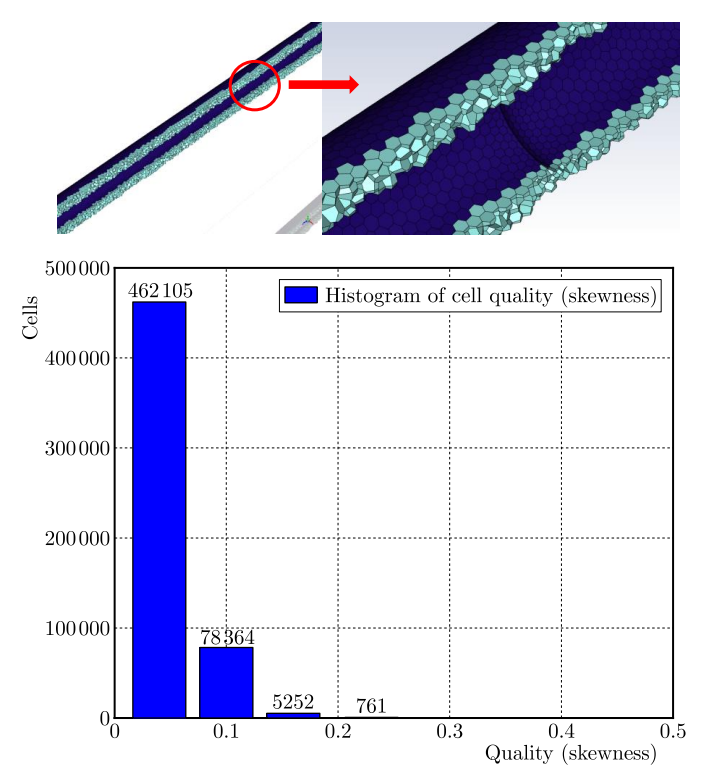


Fig. 3. Physical model and meshing of eccentric annulus with the eccentricity of 10%.

Let us set the direction of gravity as the y-axis and the direction of the ring-space axis as the z-axis. For different eccentricity models (0 %, 10 %, 20 %, 30 %, 40 %), we set different displacements:  $5 \, \text{L/s}$ ,  $8 \, \text{L/s}$ ,  $11 \, \text{L/s}$ ,  $14 \, \text{L/s}$ ,  $17 \, \text{L/s}$ . Numerical simulations were carried out by setting different speeds at different displacements:  $0 \, \text{rev/min}$ ,  $30 \, \text{rev/min}$ ,  $60 \, \text{rev/min}$ ,  $90 \, \text{rev/min}$ ,  $120 \, \text{rev/min}$ . Let us calculate the gradient of the pressure drop in the annulus of the whole model at different eccentricities and at different displacements and speeds. The gradients of pressure drop in the annulus at different combinations of drilling tools at different rotational speeds and displacements were calculated for the models with  $0 \, \%$  eccentricity and  $10 \, \%$  eccentricity. For the  $10 \, \%$  model of eccentricity, the gradient of pressure drop in the annulus was calculated with and without a drilling tool joint at different displacements.

The main simulation parameters are set as: drilling fluids set to H-B fluids. According to the performance data of drilling fluid used in the field of SY-3 well, the reference viscosity is  $0.058\,\mathrm{Pa}\cdot\mathrm{s}$ . The yield stress of drilling fluid is  $7.15\,\mathrm{Pa}$  with a Power Law Index of 0.53. The Consistency Index is 0.48. Drilling fluid is an incompressible fluid with a density set to a constant  $1400\,\mathrm{kg/m^3}$ . The reference temperature is set at  $400\,\mathrm{K}$  based on geologic information. Let us set boundaries for the inlet velocity and outlet pressure. The inlet speed is set to  $0.139\,\mathrm{m/s} - 0.556\,\mathrm{m/s}$  ( $5\,\mathrm{L/s} - 17\,\mathrm{L/s}$ ) and the rotational speed is  $0\,\mathrm{rev/min} - 120\,\mathrm{rev/min}$ . The Solver parame-

ters are configured as follows: pressure-velocity coupling using the SIMPLE scheme of predicting the velocity field and then correcting it by the pressure field. To improve the convergence speed and computational accuracy, the spatial discretization format is chosen as the second-order windward format.

# 3. Analysis of numerical simulation results

#### 3.1. Hydraulic behavior law of eccentric annulus in small wellbore

Eccentric flow fields have asymmetric flow and uneven velocity distribution compared to concentric flow fields. Furthermore, due to the small gap in the small borehole annulus, the drilling fluid is forced to rotate with the drill column due to its viscosity, causing the drilling fluid and drill cuttings spiral flow in the annulus. The flow of drilling fluid in the annulus has been changed to a spiral flow, which is shown in Fig. 4 (Delwiche *et al.*, 1992).

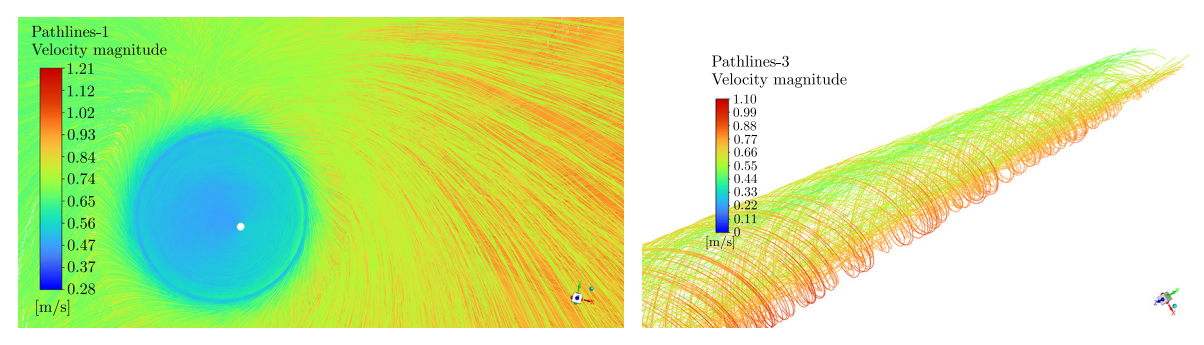


Fig. 4. Simulated slim-hole annular fluid flow trajectory diagram.

According to the existing drilling hydraulics theory (Singh et al., 2021; Miao et al., 2023), the fluid flow velocity in the eccentric annulus will not have a standard circular velocity distribution, and the overall flow velocity at the wide gap of the eccentric annulus flow field is larger than that at the narrow gap. Velocity is lower at the drill pipe and well wall contact position, and higher at the center. The flow rate at the drill pipe and well wall is zero, which is consistent with the assumption of no slip at the wall boundary. Let us take the working condition of 20% eccentricity,  $8\,\text{L/s}$  displacement and  $60\,\text{rev/min}$  as an example. Let us create a cross-section at  $12\,\text{m}$  from the model axis, in this case, a  $73\,\text{mm}$  drill pipe cross-section from the drilling tool set. The axial flow velocity cloud at this cross-section is shown in Fig. 5. Let us create a line from the narrow gap to the wide gap at each of the  $0.1\,\text{m}$  (bit),  $5\,\text{m}$  (MWD),  $12\,\text{m}$  (drill pipe), and  $15\,\text{m}$ 

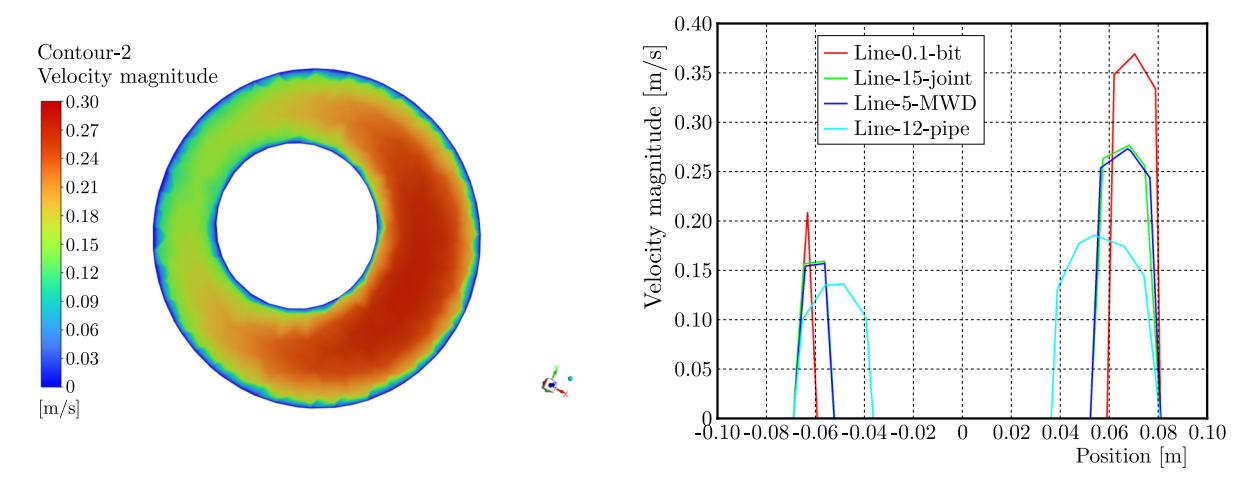


Fig. 5. Flow velocity cloud chart and distribution along the line at 12 m cross-section.

(joint) sections. The distribution of the flow velocity extending the line is obtained and plotted, and the results are shown in Fig. 5.

During the drilling fluid circulation process, the pressure distribution law of the flow field in the annulus can be basically expressed as the fluid dynamic pressure distribution law. The dynamic pressure distribution of the fluid in the annulus is similar to the velocity distribution, showing the phenomenon of low dynamic pressure at the position of fluid contacting the drill pipe and the well wall, and high dynamic pressure in the middle of the gap, and the dynamic pressure at the wide gap is larger than that at the narrow gap. The dynamic pressure cloud at 12 m section and the distribution of dynamic pressure along the line at 0.1 m (drill bit), 5 m (MWD), 12 m (drill pipe), and 15 m (joint) sections are shown in Fig. 6.

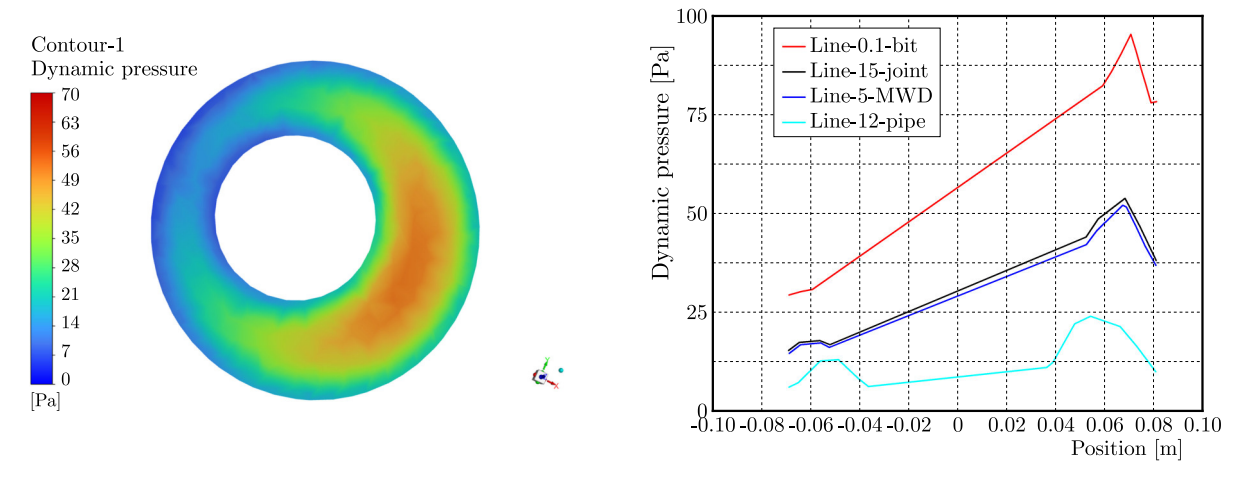


Fig. 6. Dynamic pressure cloud chart and distribution along the line at 12 m cross-section.

#### 3.2. Results of numerical simulation of pressure drop gradient in the annulus

Let us analyze the variation of static pressure along the z-axis of the fluid domain model. Let us take the working condition of 20 % eccentricity, 8 L/s displacement and 60 rev/min as an example. The simulation results for the variation of drilling fluid static pressure along the z-axis of the fluid domain model are shown in Fig. 7. It can be seen that the gradient of pressure drop in the annulus is significantly different at different combinations of drilling tools. The pressure drop gradient is maximum at the drill bit with  $560.6166 \,\mathrm{Pa/m}$  and minimum at the drill pipe with  $72.1636 \,\mathrm{Pa/m}$ .

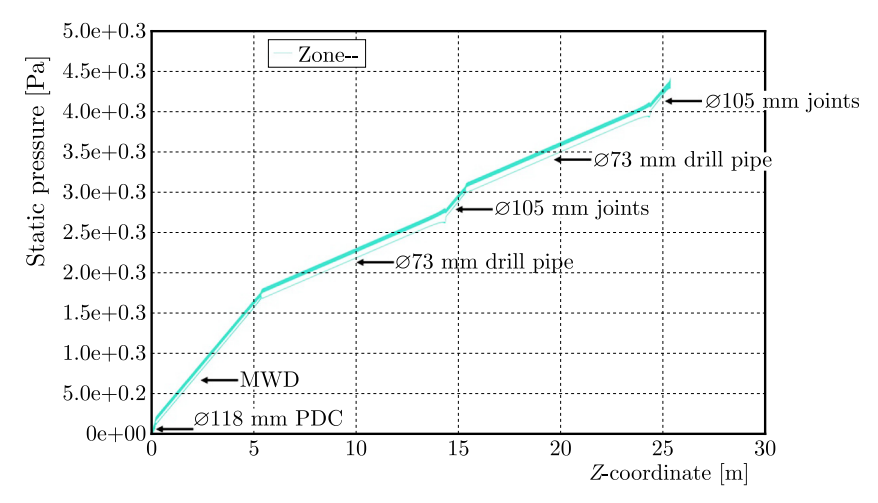


Fig. 7. Static pressure changes along the z-axis.

Let us simulate different speed conditions under different displacement for different eccentricity models. Let us record the pressure difference variation along the z-axis of the fluid domain model and calculate the pressure drop gradient. The calculation results of the annular pressure drop gradient under different models and operating conditions are shown in Tables 1–5.

Table 1. Numerical simulation results of pressure drop gradient in eccentric rotating annulus under a displacement of  $5\,\mathrm{L/s}$ .

Eccentricity [%]	Gradient of annular pressure drop at different speeds [Pa/m]							
Decembrately [70]	0 rev/min	$30\mathrm{rev/min}$	60 rev/min	90 rev/min	$120\mathrm{rev/min}$			
0	120.4681	120.5886	121.7639	115.3544	122.6413			
10	117.4402	117.9311	118.7662	113.5687	118.0307			
20	113.8847	114.4879	115.4942	111.7446	114.1889			
30	110.5325	111.5087	112.6088	110.8481	111.8028			
40	105.0750	105.7200	106.8325	104.0990	106.5690			

Table 2. Numerical simulation results of pressure drop gradient in eccentric rotating annulus under a displacement of  $8\,\mathrm{L/s}$ .

Eccentricity [%]	Gradient of annular pressure drop at different speeds [Pa/m]							
Decembrately [70]	0 rev/min	$30\mathrm{rev/min}$	$60\mathrm{rev/min}$	90 rev/min	$120\mathrm{rev/min}$			
0	202.8120	203.2494	204.5276	206.7835	210.6868			
10	196.9904	197.6563	199.2859	202.2209	206.8817			
20	192.0572	192.8892	195.1042	198.7576	202.8354			
30	183.4290	184.2530	186.3566	190.2460	192.3735			
40	202.8120	203.2494	204.5276	206.7835	210.6868			

Table 3. Numerical simulation results of pressure drop gradient in eccentric rotating annulus under a displacement of  $11 \,\mathrm{L/s}$ .

Eccentricity [%]	Gradient of annular pressure drop at different speeds [Pa/m]							
Eccentricity [70]	0 rev/min	30  rev/min $60  rev/min$ $90  rev/$		90 rev/min	$120\mathrm{rev/min}$			
0	289.9956	290.5888	292.2413	304.2785	308.9576			
10	292.2724	292.8492	294.4537	297.2361	302.2488			
20	284.2837	285.2724	287.4275	290.9739	296.9511			
30	278.0806	279.5182	282.2917	286.9200	293.9188			
40	266.3290	267.9681	270.9574	275.6357	283.1700			

Table 4. Numerical simulation results of pressure drop gradient in eccentric rotating annulus under a displacement of  $14\,\mathrm{L/s}$ .

Eccentricity [%]	Gradient of annular pressure drop at different speeds [Pa/m]							
Eccentricity [70]	0 rev/min	$30\mathrm{rev/min}$	60 rev/min	90 rev/min	$120\mathrm{rev/min}$			
0	477.7297	478.2641	479.8586	482.7228	487.5286			
10	465.3709	466.2607	467.9278	471.7419	476.8852			
20	453.3478	455.1508	457.9864	462.7643	468.4593			
30	445.0284	447.9129	452.0198	458.6739	466.1605			
40	427.8005	431.2983	436.0922	443.1240	452.7278			

Eccentricity [%]	Gradient of annular pressure drop at different speeds [Pa/m]							
Eccentricity [70]	0 rev/min	$30\mathrm{rev/min}$	$60\mathrm{rev/min}$	$90\mathrm{rev/min}$	$120\mathrm{rev/min}$			
0	596.7309	597.3693	599.2548	602.1814	607.0979			
10	581.4885	582.485	584.6119	588.5206	593.8054			
20	507.1162	569.0454	572.3498	577.2255	584.1269			
30	557.3839	560.9270	566.0114	573.1992	581.4801			
40	536.7739	541.2815	547.4001	555.9908	563.7933			

Table 5. Numerical simulation results of pressure drop gradient in eccentric rotating annulus under a displacement of  $17 \,\mathrm{L/s}$ .

# 3.3. Three-factor analysis of eccentricity, rotation, and displacement

Let us draw a four-dimensional scatter plot by combining different eccentricity models, displacement, and rotation settings with data from Tables 1–5. In Fig. 8, the x-axis represents rotational speed, y-axis represents displacement, and z-axis represents eccentricity. The scattered points' color represents the magnitude of the annular pressure drop gradient. From the scatter plot, it can be clearly seen that the pressure drop gradient in the annulus tends to increase with the increase in speed and displacement. Combining the scatter plot matrix in Fig. 9, the histogram at the diagonal position allows us to see the distribution of each variable, while the scatter plots above and below the diagonal show the relationship between variables pairwise. There is a significant monotonic relationship between displacement and the annular pressure drop gradient. The pressure drop gradient in the annulus is more significantly affected by the rotational speed at high speeds (>90 rev/min) than at low speeds. As the eccentricity increases, the pressure drop gradient in the annulus slightly decreases.

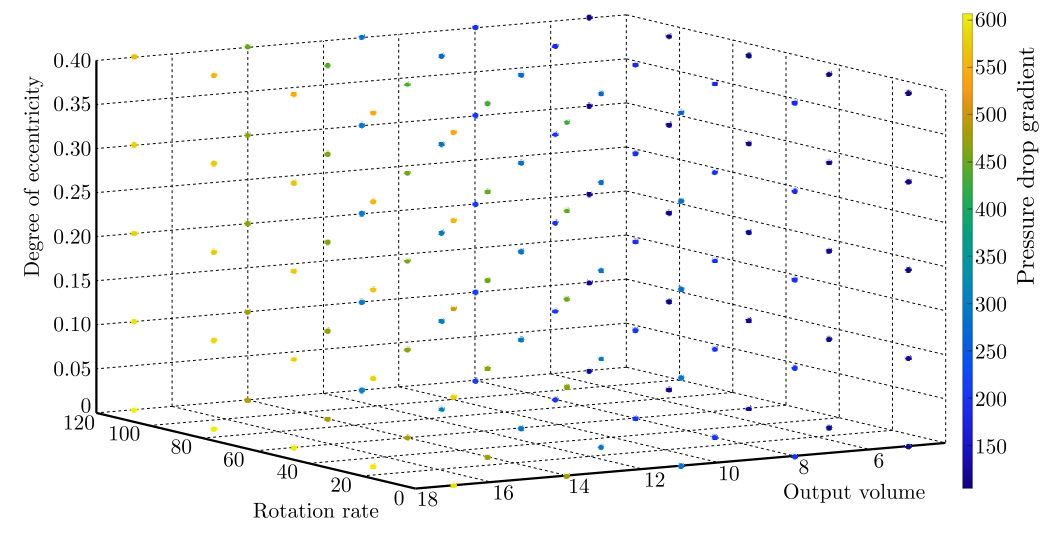


Fig. 8. Four-dimensional scatter plot analysis of three factors.

We used the coefficient comparison method in a multiple regression model to analyze the magnitude of the gradient effect of eccentricity, rotation, and displacement on the annular pressure drop (Bao & Weng, 2000; Mielke & Berry, 2002). Usually, while constructing a multifactor regression model, the equations are presented with unstandardized regression coefficients. It is the original regression coefficient corresponding to different independent variables in the equation, reflecting the magnitude of the effect of each unit change in the independent variable on the dependent variable when other factors remain constant. The variables in this article have asynchronous changes during simulation experiments. Let us standardize variables when

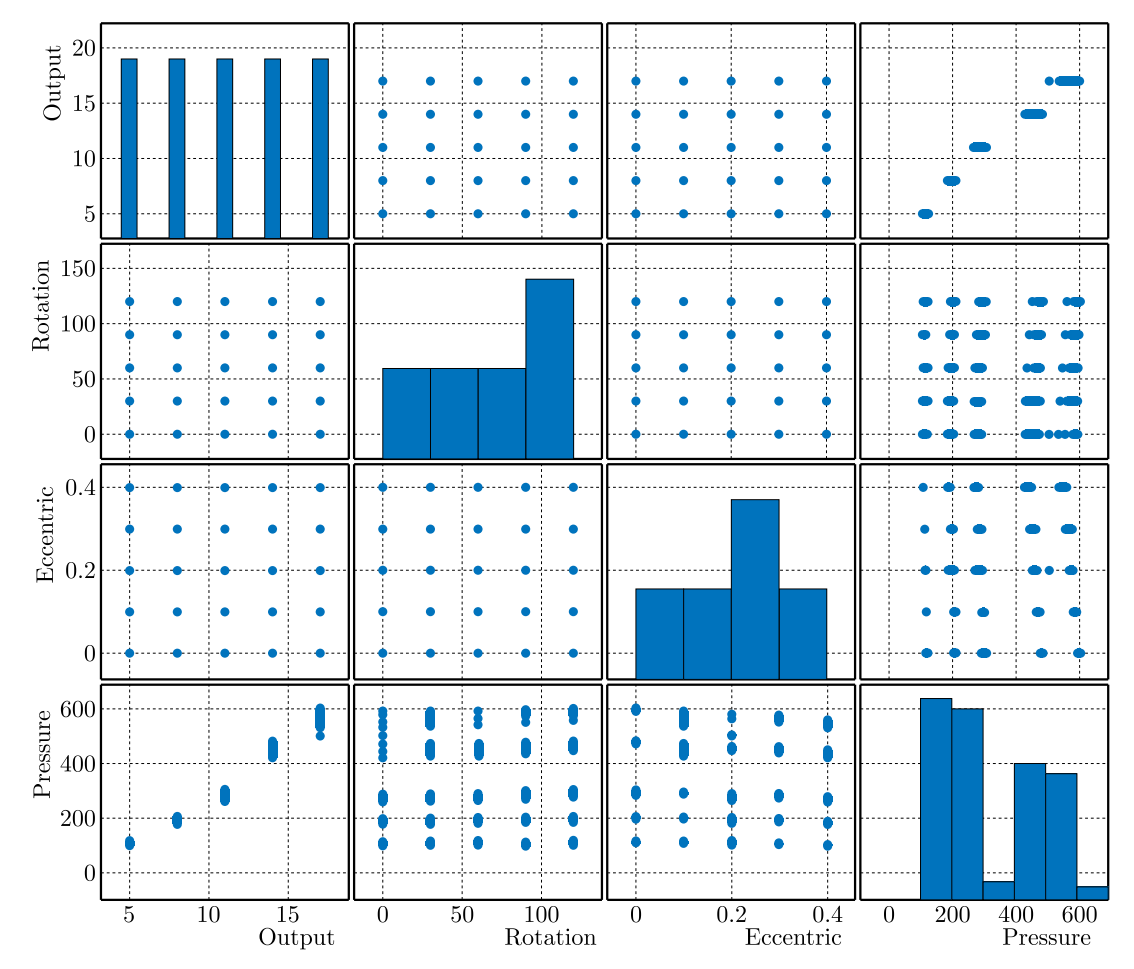


Fig. 9. Scatter plot matrix.

incorporating them into the regression model. At this point, it reflects the impact of every standard deviation change in the independent variable on the dependent variable. The standardized coefficient regression results are shown in Table 6. Through coefficient comparison, it can be seen that the effect of displacement on the annular pressure drop gradient is the most significant, while the effect of speed and eccentricity on the annular pressure drop gradient is relatively small, and eccentricity is negatively correlated with the annular pressure drop gradient.

Table 6. Normalized coefficient regression.

Coefficient									
Model	Non standardized coefficient		Standardized coefficient	t	Significance				
Wiodei	В			Significance					
Constant	-98.280	7.397	_	-13.287	1.000				
Displacement	39.345	0.509	0.988	77.267	0.000				
Speed	0.114	0.051	0.029	2.237	0.027				
Eccentricity	-72.644	15.276	-0.061	-4.755	0.000				
		Dependent variable	: pressure drop gradient	•	•				

Let us create a scatter plot of the annular pressure drop gradient with smooth lines and data labels for different speeds and eccentricities at various displacements. As shown in Fig. 10, when the displacement is less than 11 L/s and the speed is less than 60 rev/min, the pressure drop gradient in the annulus increases with the increase in speed. When the speed is greater than

60 rev/min, the pressure drop gradient in the annulus slightly decreases with increasing speed. When the speed increases to 90 rev/min or above, the pressure drop gradient in the annulus continues to rise with the increase in speed. When the displacement is  $\geq 11 \, \text{L/s}$ , the annular pressure drop gradient increases monotonically with the increase in rotational speed, and the higher the rotational speed, the greater the impact on the annular pressure drop gradient. When the eccentricity is less than 0.3 and the displacement is greater than 14 L/s, the pressure drop gradient in the annulus at low speed initially increases and then decreases with the increase in eccentricity. The overall trend is that the annular pressure drop gradient decreases with increasing eccentricity, and the larger the eccentricity, the greater the impact on the annular pressure drop gradient. Among them, when the displacement is 5 L/s and the speed is 90 rev/min, all eccentricity model annular pressure drop gradients show a decreasing trend. The eccentricity 0.4 model achieves the lowest annular pressure drop gradient at this displacement at this speed. At a displacement of 11 L/s, the annular pressure drop gradient of the model with 0 eccentricity is smaller than that of the model with 0.1 eccentricity before reaching 60 rev/min. At speeds of 90 rev/min and above, the annular pressure drop gradient of the model with 0 eccentricity increases faster, surpassing the model with 0.1 eccentricity. At a displacement of 17 L/s, the model with an eccentricity of 0.2 obtains the minimum annular pressure drop gradient at a speed of 0 rev/min.

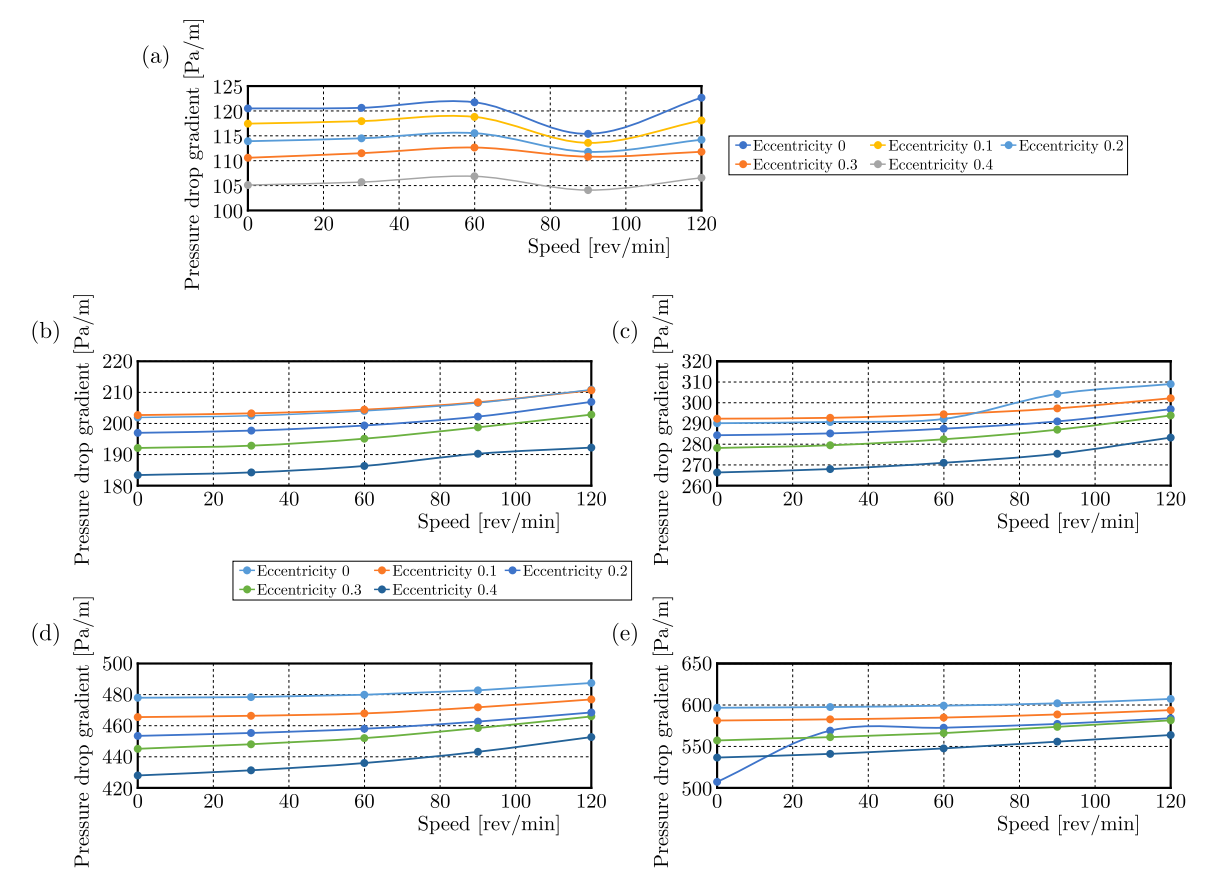


Fig. 10. Pressure drop gradient in the annulus under different speeds and eccentricities with displacements of:

(a) 5 L/s; (b) 8 L/s; (c) 11 L/s; (d) 14 L/s; (e) 17 L/s.

# 3.4. Differences in pressure drop gradients in the annulus for different combinations of drilling tools

Let us create a pipe string model through Solidworks to explore the annular pressure loss of different drilling tool combinations. Using eccentricity 0 and eccentricity 0.1 models as simulation experimental objects, let us record the pressure difference between the upper and lower sections of

each drilling tool, and obtain the annular pressure drop gradient. Let us analyze the differences in the annular pressure drop gradient at different drilling tool combinations under different displacements, eccentricities, and speeds. The simulation experiments are shown in Tables 7–11.

Table 7. Calculation results of annular pressure drop gradient at different drilling tools under  $5\,\mathrm{L/s}$  displacement.

Different eccentricity models	Different simulated drilling tools	The pressure drop gradient in the annulus at different rotational speeds [Pa/m]					
eccentricity models	drining tools	at different rotational speeds 0 rev/min   30 rev/min   60 rev/min   90 rev it   577.2046   566.7762   545.4048   527. 0   234.1352   232.7951   231.9452   230. 0   239.2424   241.3771   248.4087   265. 0   72.6384   72.8911   73.4337   65.8 0   246.8312   224.2789   222.2801   219. 0   231.0896   234.1507   239.8133   257.	90 rev/min	$120\mathrm{rev/min}$			
	Simulated drill bit	577.2046	566.7762	545.4048	527.0940	509.5932	
Eccentricity 0	Simulated MWD	234.1352	232.7951	231.9452	230.0234	228.5605	
	Simulated joint	239.2424	241.3771	248.4087	265.7412	288.5091	
	Simulated drill pipe	72.6384	72.8911	73.4337	65.8288	73.8904	
	Simulated drill bit	568.2580	560.6166	541.1510	514.6571	510.2580	
Eccentricity 0.1	Simulated MWD	246.8312	224.2789	222.2801	219.8526	218.8613	
Decembricity 0.1	Simulated joint	231.0896	234.1507	239.8133	257.5202	276.3035	
	Simulated drill pipe	71.8530	72.1636	72.7504	66.2534	70.37980	

Table 8. Calculation results of annular pressure drop gradient at different drilling tools under 8 L/s displacement.

Different eccentricity models	Different simulated drilling tools	The pressure drop gradient in the annulus at different rotational speeds [Pa/m]					
eccentricity models	drining tools	$0\mathrm{rev/min}$	$30\mathrm{rev/min}$	$60\mathrm{rev/min}$	90 rev/min	$120\mathrm{rev/min}$	
	Simulated drill bit	980.4990	971.7729	946.0966	908.8517	866.2889	
Eccentricity 0	Simulated MWD	393.8126	393.3917	392.1140	390.5879	388.8704	
	Simulated joint	401.6579	404.1619	411.9381	426.0342	449.4999	
	Simulated drill pipe	121.6249	121.7959	122.8887	124.7786	129.9980	
	Simulated drill bit	1000.1140	992.7490	970.9457	940.6719	913.6777	
Eccentricity 0.1	Simulated MWD	377.1419	376.7523	375.4036	372.9664	373.2648	
	Simulated joint	392.2802	394.2948	401.0442	413.8018	432.2522	
	Simulated drill pipe	127.7627	128.0762	129.0871	131.9266	133.1912	

Table 9. Calculation results of annular pressure drop gradient at different drilling tools under  $11\,\mathrm{L/s}$  displacement.

Different eccentricity models	Different simulated drilling tools	The pressure drop gradient in the annulus at different rotational speeds [Pa/m]					
eccentricity models	drining tools	0 rev/min	$30\mathrm{rev/min}$	$60\mathrm{rev/min}$	90 rev/min	$120\mathrm{rev/min}$	
	Simulated drill bit	1486.7360	1480.1770	1459.6640	1428.7510	1394.7340	
Eccentricity 0	Simulated MWD	535.3307	535.1713	534.5935	533.6185	533.1697	
	Simulated joint	560.3379	560.8369	569.6386	582.5776	604.7408	
	Simulated drill pipe	186.9023	187.2892	188.5602	190.5277	194.7520	
	Simulated drill bit	1455.2450	1447.1880	1422.6190	1427.3020	1383.2950	
Eccentricity 0.1	Simulated MWD	559.1121	558.8473	557.9023	556.9548	556.3359	
Eccentricity 0.1	Simulated joint	573.2401	576.1122	584.0520	602.3688	624.3576	
	Simulated drill pipe	176.7335	176.9028	178.1618	191.8827	195.6730	

Simulated drill pipe

Different eccentricity models	Different simulated drilling tools	The pressure drop gradient in the annulus at different rotational speeds [Pa/m]					
eccentricity models	drining tools	0 rev/min	$30\mathrm{rev/min}$	$60\mathrm{rev/min}$	90 rev/min	$120\mathrm{rev/min}$	
	Simulated drill bit	2535.1230	2528.229	2506.491	2472.6240	2425.1050	
Eccentricity 0	Simulated MWD	881.3331	881.1474	880.4879	880.0918	879.4367	
	Simulated joint	920.9313	923.4875	930.8826	942.2473	962.8600	
	Simulated drill pipe	303.7599	304.1637	305.1402	306.6544	310.4984	
	Simulated drill bit	2524.9240	2520.2230	2501.6560	2473.846	2437.0160	
Eccentricity 0.1	Simulated MWD	842.1706	842.5658	842.0543	843.0256	843.4042	
	Simulated joint	889.7953	892.5088	899.2022	912.9028	933.2046	

Table 10. Calculation results of annular pressure drop gradient at different drilling tools under 14 L/s displacement.

Table 11. Calculation results of annular pressure drop gradient at different drilling tools under  $17\,\mathrm{L/s}$  displacement.

300.9917

302.2901

305.2190

309.4928

300.3946

Different eccentricity models	Different simulated drilling tools	The pressure drop gradient in the annulus at different rotational speeds [Pa/m]					
eccentricity models	drining tools	0 rev/min	$30\mathrm{rev/min}$	$60\mathrm{rev/min}$	$90\mathrm{rev/min}$	$120\mathrm{rev/min}$	
	Simulated drill bit	3297.4322	3291.0201	3271.5220	3238.6260	3194.9181	
Eccentricity 0	Simulated MWD	1096.8991	1096.7751	1096.8383	1096.3944	1096.0871	
	Simulated joint	1151.0115	1153.6450	1161.0901	1172.8780	1193.5186	
	Simulated drill pipe	380.0268	380.6023	381.8937	383.9324	388.3010	
	Simulated drill bit	3286.5050	3282.4980	3266.0181	3240.2089	3206.3397	
Eccentricity 0.1	Simulated MWD	1048.6480	1049.1877	1049.0842	1050.1278	1052.3933	
Eccentricity 0.1	Simulated joint	1112.9489	1115.7730	1123.3630	1137.1562	1156.3222	
	Simulated drill pipe	375.9475	376.6142	378.4151	381.8080	384.9924	

According to the simulated calculation data, it can be seen that the annular pressure drop gradient at the drill bit is the largest and the annular pressure drop gradient at the drill rod is the smallest. This is because the size of the drill bit is larger than that of the drill rod, resulting in a smaller annular clearance, faster flow velocity, and higher dynamic pressure on the crosssection. However, in actual drilling, due to the overall length of the drill pipe being much longer than the drill bit, the main annular pressure loss is still distributed at the drill pipe. The size set by MWD in the simulation is larger than that of the drilling tool joint. The pressure drop gradient in the annulus at the MWD is greater than that at the joint of the drilling tool only in the 0.1 eccentricity model, when simulating working conditions at 5 L/s and 0 rev/min speed. In the overall trend, the pressure drop gradient in the annulus at the MWD is smaller than that in the drilling tool joint. Moreover, as the displacement and speed increase, the difference becomes greater. This is mainly because the MWD length is greater than that of the drilling tool joint, and the diameter change of the drilling tool near the MWD is smaller, while the diameter change at the drilling tool joint is more obvious, and the fluid is more affected. This indicates that in actual drilling, the impact of drilling tool joints or sudden diameter changes on annular pressure loss is difficult to ignore. Let us explore the influence of drilling tool joints on annular pressure loss based on the 0.1 eccentricity model. Let us simulate the difference in the annular pressure drop gradient with and without joints at different displacements at 0 rev/min. The simulation results are shown in Fig. 11. From the figure, it can be seen that the difference in the annular pressure drop gradient between the joint and the non-joint is over 200%,

and even more than three times at a displacement of  $5 \,\mathrm{L/s}$ . Furthermore, as the displacement increases, the impact of the joint on the annular pressure drop gradient becomes greater.

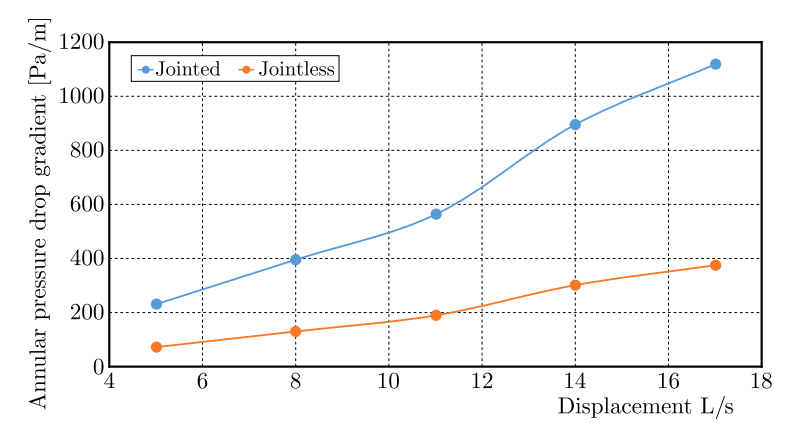


Fig. 11. Pressure drop gradient in annular space with and without joints at different displacements.

### 4. Fitting correction factors and validation

Let us divide the annular pressure drop gradient data in Tables 1–5 by the annular pressure drop gradient at a concentric non-rotating 8 L/s displacement to obtain the dimensionless annular pressure drop gradient. Let us perform multivariate fitting to obtain the multivariate fitting formula:

$$\Delta P_N = -0.487 + 0.195V + 0.001R - 3.6E, \tag{4.1}$$

where  $\Delta P_N$  is the dimensionless annular pressure drop gradient factor, V is the displacement, R is the speed, and E is the eccentricity.

Based on the historical data of the SY-3 well, a horizontal section of the SY-3 well was selected as the calculation point for lateral drilling. The drilling tool combination consisted of  $\emptyset$ 118 mm PDC +  $\emptyset$ 95 mm Screw drilling tools (1.5°) +  $\emptyset$ 103 mm non-magnetic drill pipe + directional joint + 103 mm non-magnetic drill pipe +  $\emptyset$ 73 mm weighted drill pipe + hydraulic oscillator  $+\varnothing73\,\mathrm{mm}$  weighted drill pipe  $+\varnothing73\,\mathrm{mm}$  drill pipe  $+\varnothing73\,\mathrm{mm}$  weighted drill pipe  $+ \varnothing 73 \,\mathrm{mm}$  drill pipe. Drilling fluid density is  $1400 \,\mathrm{kg/m^3}$ , viscosity is  $0.058 \,\mathrm{Pa \cdot s}$ , displacement is 7 L/s, speed is 40 rev/min. At this time, the pump pressure is 23 Mpa. Based on the rheological properties of drilling fluid and the size of the flow channel, the pressure drop gradient  $\Delta P$  of the H-B fluid annulus under concentric non-rotating 8 L/s displacement is obtained through an analytical formula. Based on the characteristics of the wellbore section such as the inclination angle, slope angle, and drill string size, the eccentricity E is determined using the drill string buckling theory (Vaughn, 1965; Juvkam-Wold & Wu, 1992; Lubinski & Althouse, 1962; Dawson, 1984; Tian et al., 2024). Let us calculate the dimensionless annular pressure drop gradient factor based on Eq. (4.1) for displacement V and speed R, and correct  $\Delta P$ . The system's cyclic pressure loss was calculated based on the well history data. Besides, the error was less than 10% when compared with the annular pressure loss calculated by the fitting model. This validates the accuracy of the model.

#### 5. Conclusions

- After analyzing the hydraulic behavior of eccentric rotating annular fluid in a small well-bore through Fluent simulation, the overall flow velocity at the wide gap of the eccentric annular flow field was found to be greater than that at the narrow gap. The speed is lower at the contact position between the drill pipe and the wellbore wall, but higher at the center. The dynamic pressure distribution and velocity distribution characteristics of the fluid

- in the annulus are similar, showing a phenomenon of low dynamic pressure at the contact position between the fluid and the drill pipe and wellbore while high dynamic pressure is observed in the middle of the gap.
- The gradient of annular pressure drop was obtained through simulation calculation results. A comprehensive analysis was conducted on the three factors affecting annular pressure loss, namely eccentricity, rotation, and displacement. At low speeds, the annular pressure drop gradient first increases and then decreases with increasing eccentricity, but overall there is a trend of the annular pressure drop gradient decreasing with increasing eccentricity. The greater the eccentricity, the greater the impact of eccentricity on the pressure drop gradient in the annulus.
- The annular pressure drop gradient was simulated and calculated with different drilling tool combinations. The differences were analyzed in the annular pressure drop gradient at different drilling tool combinations under different displacements, eccentricities, and speeds. The impact of drilling tool joints on annular pressure loss was explored. As the displacement increases, the impact of the joint on the annular pressure drop gradient becomes greater.
- Multi factor fitting of the dimensionless annular pressure drop gradient factor was analyzed through numerical simulation results. The pump pressure of a certain lateral drilling horizontal section of SY-3 well was analyzed and combined with well history data. The prediction error is less than 10%, which verifies the accuracy of the model.

#### References

- 1. Bao, F.D., & Weng, X.H. (2000). The software solving of multiple regression and correlation analysis and case explanation (in Chinese). *Journal of Applied Statistics and Management*, 20(5), 56–61.
- 2. Cartalos, U., King, I., Dupuis, D., & Sagot, A. (1996). Field validated hydraulic model predictions give guidelines for optimal annular flow in slimhole drilling. In *IADC/SPE Drilling Conference* (Article SPE-35131-MS). Society of Petroleum Engineers. https://doi.org/10.2118/35131-MS
- 3. Dawson, R. (1984). Drill pipe buckling in inclined holes. *Journal of Petroleum Technology*, 36(10), 1734–1738. https://doi.org/10.2118/11167-PA
- 4. Delwiche, R.A., Lejeune, M.W.D., Mawet, P.F.B.N., & Vignette, R. (1992). Slimhole drilling hydraulics. In *SPE Annual Technical Conference and Exhibition* (Article SPE-24596-MS). Society of Petroleum Engineers. https://doi.org/10.2118/24596-MS
- 5. Enfis, M., Ahmed, R., & Saasen, A. (2011). The hydraulic effect of tool-joint on annular pressure loss. In *SPE Production and Operations Symposium* (Article SPE-142282-MS). Society of Petroleum Engineers. https://doi.org/10.2118/142282-MS
- Haciislamoglu, M., & Cartalos, U. (1994). Practical pressure loss predictions in realistic annular geometries. In SPE Annual Technical Conference and Exhibition (Article SPE-28304-MS). Society of Petroleum Engineers. https://doi.org/10.2118/28304-MS
- 7. Hansen, S.A., Rommetveit, R., Sterri, N., Aas, B., & Merlo, A. (1999). A new hydraulics model for slim hole drilling applications. In SPE/IADC Middle East Drilling Technology Conference (Article SPE-57579-MS). Society of Petroleum Engineers. https://doi.org/10.2118/57579-MS
- 8. Hemphill, T., & Ravi, K. (2005). Calculation of drillpipe rotation effects on fluids in axial flow: An engineering approach. In *SPE Annual Technical Conference and Exhibition* (Article SPE-97158-MS). Society of Petroleum Engineers. https://doi.org/10.2118/97158-MS
- 9. Juvkam-Wold, H.C., & Wu, J. (1992). Casing deflection and centralizer spacing calculations. Society of Petroleum Engineers Drilling Engineering, 7(4), 268–274. https://doi.org/10.2118/21282-PA
- 10. Kelessidis, V.C., Dalamarinis, P., & Maglione, R. (2011). Experimental study and predictions of pressure losses of fluids modeled as Herschel–Bulkley in concentric and eccentric annuli in laminar, transitional and turbulent flows. *Journal of Petroleum Science and Engineering*, 77(3–4), 305–312. https://doi.org/10.1016/j.petrol.2011.04.004

11. Khatibi, M., Wiktorski, E., Sui, D., & Time, R.W. (2018). Experimental study of frictional pressure loss for eccentric drillpipe in horizontal wells. In *IADC/SPE Asia Pacific Drilling Technology Conference and Exhibition* (Article SPE-191046-MS). Society of Petroleum Engineers. https://doi.org/10.2118/191046-MS

- 12. Letelier, M.F., Siginer, D.A., & Hinojosa, C.B. (2017). On the physics of viscoplastic fluid flow in non-circular tubes. *International Journal of Non-Linear Mechanics*, 88, 1–10. https://doi.org/10.1016/j.ijnonlinmec.2016.09.012
- 13. Lubinski, A., & Althouse, W.S. (1962). Helical buckling of tubing sealed in packers. *Journal of Petroleum Technology*, 14(6), 655–670. https://doi.org/10.2118/178-PA
- 14. McCann, R.C., Quigley, M.S., Zamora, M., & Slater, K.S. (1995). Effects of high-speed pipe rotation on pressures in narrow annuli. *Society of Petroleum Engineers Drilling & Completion*, 10(2), 96–103. https://doi.org/10.2118/26343-PA
- 15. Miao, H., Dokhani, V., Ma, Y., & Zhang, D. (2023). Numerical modeling of laminar and turbulent annular flows of power-law fluids in partially blocked geometries. *Results in Engineering*, 17, Article 100930. https://doi.org/10.1016/j.rineng.2023.100930
- 16. Mielke, P.W., & Berry, K.J. (2002). Multivariate multiple regression analyses: A permutation method for linear models. *Psychological Reports*, 91(1), 3–9. https://doi.org/10.2466/pr0.2002.91.1.3
- 17. Reed, T.D., & Pilehvari, A.A. (1993). A new model for laminar, transitional, and turbulent flow of drilling muds. In *SPE Production Operations Symposium* (Article SPE-25456-MS). Society of Petroleum Engineers. https://doi.org/10.2118/25456-MS
- 18. Resell, Å.Aa., Giljarhus, K.E.T., Mihai, R., & Skadsem, H.J. (2025). Fluid forces in eccentric annular geometries with rotating and orbiting inner cylinder. *Physics of Fluids*, 37(4), Article 047158. https://doi.org/10.1063/5.0262548
- 19. Shi, K., & Zhang, S. (2025). Turbulent transport in annular Poiseuille flow with axial rotation. *Physics of Fluids*, 37(3), Article 035116. https://doi.org/10.1063/5.0257318
- 20. Singh, R., Ahmed, R., Karami, H., Nasser, M., & Hussein, I. (2021). CFD analysis of turbulent flow of power-law fluid in a partially blocked eccentric annulus. *Energies*, 14(3), Article 731. https://doi.org/10.3390/en14030731
- 21. Song, Z.C., Wang, G.C., Guan, Z.C., & Zou, D.Y. (2004). A method for computing the circulating pressure loss in slim hole annulus (in Chinese). *Petroleum Drilling Techniques*, 32(6), 11–12.
- 22. Sotoudeh, S., Frigaard, I.A. (2024). Computational study of Newtonian laminar annular horizontal displacement flows with rotating inner cylinder. *Physics of Fluids*, 36(8), Article 083113. https://doi.org/10.1063/5.0222314
- 23. Tian, J., Song, H., Yang, Y., Mao, L., & Song, J. (2024). Dynamic buckling characteristics of drill string in horizontal wells. *International Journal of Structural Stability and Dynamics*, 24(11), Article 2450121. https://doi.org/10.1142/S0219455424501219
- 24. Tian, Y., Jiang, D.L., Ma, C.H., Xu, Y.L., Yu, X.D., & Song, X.C. (2022). Numerical simulation of the effects of eccentric rotation of the drill string on annular frictional pressure drop (in Chinese). *Petroleum Drilling Techniques*, 50(5), 42–49. https://doi.org/10.11911/syztjs.2022104
- 25. Vaughn, R.D. (1965). Axial laminar flow of non-Newtonian fluids in narrow eccentric annuli. *Society of Petroleum Engineers Journal*, 5(4), 277–280. https://doi.org/10.2118/1138-PA
- Vieira Neto, J.L., Martins, A.L., Ataíde, C.H., & Barrozo, M.A.S. (2014). The effect of the inner cylinder rotation on the fluid dynamics of non-Newtonian fluids in concentric and eccentric annuli. Brazilian Journal of Chemical Engineering, 31(4), 829–838. https://doi.org/10.1590/0104-6632.2014 0314s00002871